Squeezed Magnons-Induced Nonreciprocal Entanglement in a Magnomechanical Cavity

Ziyad Imara,^{1,*} Khadija El Anouz,^{1,†} İlkay Demir,^{2,3,‡} and Abderrahim El Allati^{1,§}

Magnomechanical cavities offer a new frontier in quantum electrodynamics that give rise to several significant theoretical and experimental results. In this paper, we propose a novel theoretical mechanism for achieving a nonreciprocal macroscopic entanglement between magnons, photons and phonons, based on the use of an alternative squeezed magnons method. Indeed, in contrast to conventional approaches, we show how precise control of the amplitude and phase of the squeezed mode allows to obtain a tunable nonreciprocity of entanglement. The magnons resulting from the collective motion of the spin in a macroscopic ferrimagnet become coupled to the microwave photons via magnetic dipole interaction and to the phonons via magnetostrictive interaction. Moreover, we establish that the proposed scheme achieves ideal nonreciprocity, which can be optimized by cavity-magnon coupling and bath temperature control. Finally, by using the parameters that are experimentally feasible with current technologies, this work provides new perspectives for hybrid magnon-based quantum technologies.

I. INTRODUCTION

The field of Magnonomechanics (MM) emerges as a highly promising platform for exploring macroscopic quantum effects [1–4]. It consists of investigating the interaction between spin waves (magnons) and mechanical vibrations (phonons) via magnetostrictive coupling [5]. These systems mainly exploit yttrium-iron garnet (YIG), a material exhibiting remarkable magnetic properties that are proving key to advanced magnetooptical applications. In fact, across various geometries, including sphere [2, 6, 7], thin film [8] or bridge [9– 11], the YIG system enables efficient magnon-phonon coupling through magnetostrictive force. Remarkably, these systems have theoretically show the ability to achieve photon-magnon-phonon entanglement, paving the way for breakthrough applications in quantum technologies, notably in information storage, ultrasensitive detection, quantum transduction, and hybrid quantum networks [12–15]. However, it has been shown that the magnons in YIG can achieve strong coupling with microwave photons in a high-quality cavity [16]. This gives rise to magnon-cavity polaritons through the collective excitations of a large number of spins [17]. Moreover, squeezed magnons are a powerful tool for improving the performance of magnomechanical systems, enhancing quantum entanglement, supporting nonlinearity to be amplified and cooling of the ground state to be improved [18, 19]. Various methods can be used to achieve magnonic squeezing; including the intrinsic nonlinearity of the magnetostriction [20, 21], reservoir-engineered

cavity magnomechanics [22], two-tone driving of a qubit [23], etc [24–26].

Notably, it has been demonstrated that the MM systems are able to achieve nonreciprocal entanglement between photons and magnons, enabled by breaking Lorentz symmetry [27]. Recently, the nonreciprocity observed in MM systems has been demonstrated by exploiting effects that induce a frequency shift in magnon resonances. This is analogous to the optomechanical Sagnac effect, and to recent developed optomechanical resonators [28–30]. In this inspiration, several approaches have been proposed to study the nonreciprocity, in particular using Kerr effect [31], achieved by spinning the MM cavity [32, 33], tuning the magnetic field orientation along the crystallographic axis of the magnon mode [34], exploiting a chiral coupling [35, 36], or via using the so-called Barnett effect [37, 38]. In this paper, we propose an alternative approach to achieve nonreciprocal entanglement, based on squeezing magnons. Our approach exploits squeezed magnon mode in a MM system to enable fine-tuning of nonreciprocity via manipulating the squeezed amplitude and phase parameters. Hence, this enable us to achieve a directional control of positive and negative frequency shifts. In contrast to conventional approaches, squeezing magnon method allows the magnon frequency and dissipation properties to be manipulated simultaneously via phase-dependent amplitude tuning. We further analyze the role of temperature and cavity-magnon coupling those enable the ideal nonreciprocal entanglement induced by this squeezing dynamics.

The present paper is structured as follows. In Sec. II, we present the theoretical model of the system, where we derive the linearized quantum Langevin equations of the system. In Sec. III, we perform numerical simulations using experimentally accessible parameters to showed the nonreciprocity of bipartite and tripartite en-

¹Laboratory of R&D in Engineering Sciences, Faculty of Sciences and Techniques Al-Hoceima, Abdelmalek Essaadi University, Tetouan, Morocco

²Department of Nanotechnology Engineering, Sivas Cumhuriyet University, 58140 Sivas, Türkiye ³Sivas Cumhuriyet University Nanophotonics Application and Research Center-CÜNAM, 58140 Sivas, Türkiye

^{*} imara.zivad@etu.uae.ac.com

[†] kelanouz@uae.ac.ma

[‡] idemir@cumhuriyet.edu.tr

[§] eabderrahim@uae.ac.ma

tanglement, followed by a detailed discussion of the results. Finally, Sec. IV summarizes the main results of our paper.

II. MODEL AND DYNAMICAL HAMILTONIAN

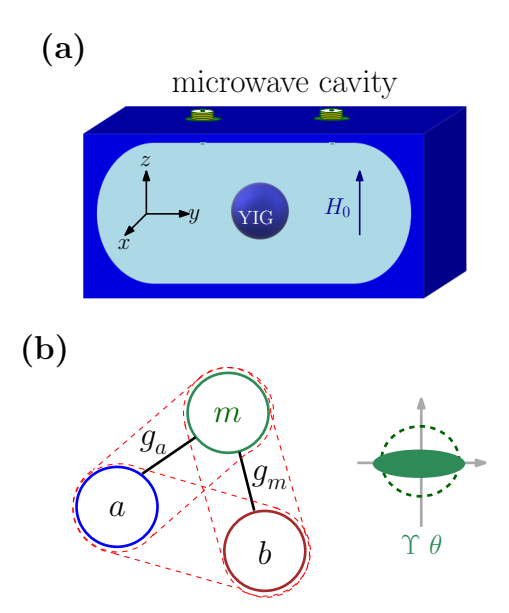


FIG. 1: (a) Schematic of the magnomechanical system with a YIG sphere in a polarizing magnetic field. A polished YIG sphere is placed inside a microwave cavity close to the maximum magnetic field region of the cavity mode. (b) Schematic of all possible bipartite entanglement and couplings model with photon-magnon (g_a) and magnon-phonon (g_m) couplings. Modes a, m and b, represent cavity, magnon, phonon respectively. Green ellipse indicates magnon mode squeezing with parameter Υ and phase θ , enabling nonreciprocal entanglement.

We consider a hybrid magnomechanical system consisting of a 250μ m-diameter YIG sphere positioned at an amplitude belly of a microwave cavity [2, 5], as shown in Fig.1. This system couples microwave photons from the cavity, magnons and phonons. The magnons interact with the phonons via magnetostrictive coupling, which induces geometrical deformation in the YIG sphere and modifies its vibrational modes [39, 40]. Thus, it establishes a mutual interaction in which the mechanical vibrations of the sphere also modify the properties of the magnons and photons in the cavity [41]. It worth mentioning that the radiation pressure effects can be neglected, when the YIG sphere is much smaller than the microwave wavelength. The Hamiltonian of the system is given as $(\hbar=1)$

$$\begin{split} \mathbf{H} &= \ \omega_a a^\dagger a + \omega_m m^\dagger m + \frac{\omega_b}{2} (q^2 + p^2) + g_m m^\dagger m q \\ &+ \ g_a (a^\dagger + a) (m^\dagger + m) + i [\Omega_0 m^\dagger e^{-i\omega_0 t} + \frac{\Upsilon}{2} m^{\dagger 2} e^{i\theta} \end{split}$$

$$- H.c], (1)$$

where $a(a^{\dagger})$ and $m(m^{\dagger})$ are the annihilation (creation) operators of the cavity mode and the magnon mode, respectively. Furthermore, $\mathcal{O} \equiv a, m$ satisfies $[\mathcal{O}, \mathcal{O}^{\dagger}] = 1$. For the mechanical vibration modes, $q = (b^{\dagger} + b)/\sqrt{2}$ and $p = i(b^{\dagger} - b)/\sqrt{2}$ are the dimensionless quadratures of position and momentum, where b (b^{\dagger}) is the annihilation (creation) operator of the j^{th} phonon mode, where [q,p]=i is satisfied. However, ω_a (ω_b) denotes the frequency of the microwave cavity (the phonon) mode. Moreover, to excite and generate the magnon mode, both YIG sphere are usually placed in a uniformly biased magnetic field H_0 . Moreover, the microwave field with its magnetic component H_a is perpendicularly applied to the polarization field [42-44].

In addition, ω_m is the frequency of the magnon mode given by means of the external bias magnetic field and the gyromagnetic ratio γ as $\omega_m = \gamma H_0$, where $\gamma/2\pi = 28 \text{GHz/T}$. However, g_a is the cavitymagnon coupling strength that can achieve the strong coupling regime for $g_a > \kappa_a \kappa_m$ [42, 43]. g_m is the magnon-phonon coupling strength and is typically small [1, 2, 5, 45]. Moreover, under the assumption of the low-lying excitations, we have $\langle m^{\dagger}m\rangle \ll 2N_0 s$, where s = 5/2 is the spin number of the ground state Fe³⁺ ion in YIG. Here, $N_0=\rho V$ is the total number of spins, with $\rho=4.22\times 10^{27}m^{-3}$ being the spin density and the volume V of the YIG-sphere. Moreover, note that the magnon mode can be driven by a charged microwave field using, e.g., a loop antenna [46]. The Rabi frequency associated with the microwave drive is governed by $\Omega_0 = \frac{\sqrt{5}}{4} \gamma \sqrt{N_0} H_d$. Finally, the last term in the Hamiltonian (1), $i(\Upsilon/2m^{\dagger 2}e^{i\theta} - \text{h.c.})$ denotes the magnon squeezing interaction, characterized by the squeezing parameters, namely Υ and θ . This magnon squeezing can be achieved by various experimental approaches, e.g., transferring the squeezing of a cavity with a squeezing vacuum field [25, 26], applying two-tone microwave fields to drive the magnon mode [23], exploiting of the magnetic anisotropy of ferromagnets [47], or by using of magnetostriction nonlinearity [18, 19].

By including the dissipative and input noise terms for each mode under the rotating-wave-approximation, namely $g_a(a+a^{\dagger})(m+m^{\dagger}) \rightarrow g_a(am^{\dagger}+ma^{\dagger})$, using the drive frequency ω_0 . Then, one can obtain the set of quantum Langevin equations (QLEs) for the system as follows

$$\dot{a} = -(i\Delta_a + \kappa_a)a - ig_a m + \sqrt{2\kappa_a}a_{\rm in},$$

$$\dot{m} = -(i\Delta_m + \kappa_m)m - ig_a a + \Omega_0 - ig_m mq + \Upsilon m^{\dagger} e^{i\theta} + \sqrt{2\kappa_m}m_{\rm in},$$

$$\dot{q} = \omega_b p , \quad \dot{p} = -\omega_b q - \gamma_b p - g_m m^{\dagger} m + \xi,$$
(2)

where $\Delta_a = \omega_a - \omega_0$, $\Delta_m = \omega_m - \omega_0$. κ_m is the intrinsic decay rate of the magnon mode, and γ_b is the damping rate of the phonon mode. Moreover, o^{in} is the

input noise operator of mode o = (a, m), which has zero mean [48]. In fact, it is characterized by the following correlation functions

$$\langle o^{in\dagger}(t)o^{in}(t'); o^{in}(t)o^{in\dagger}(t')\rangle = (\bar{n}_o; \bar{n}_o+1)\delta(t-t').$$
 (3)

Moreover, ξ is the Brownian noise operator of the mechanical mode with zero mean value $\langle \xi \rangle = 0$. In the Markov approximation, this correlation function for a mechanical mode with high quality factor $\mathcal{Q} \gg 1$ takes the form [49]

$$\langle \xi(t)\xi(t') + \xi(t')\xi(t) \rangle / 2 = \gamma_b(2\bar{n}_b + 1)\delta(t - t'), \quad (4)$$

where $\bar{n}_o = (\exp(\hbar\omega_o/(k_BT))+1)^{-1}$ denoting the mean thermal occupation number of the o-mode (o=a,m,b) at bath temperature T and the Boltzmann constant k_B [50].

Using strong coherent driving fields on the cavity and magnon modes leads to large steady-state amplitudes $|a_s|,|m_s|\gg 1$. Thus, one should linearize the QLEs in Eq. (2) around the steady-state value \mathcal{X}_s as $\mathcal{X}=\mathcal{X}_s+\tilde{\mathcal{X}}$, where $\mathcal{X}=a,m,q,p$, and neglecting the second order fluctuation terms. Indeed, the linearized QLEs describe the quantum fluctuations of the system using the quadrature fluctuation operators $(\tilde{I}_a,\tilde{J}_a,\tilde{I}_m,\tilde{J}_m,\tilde{q},\tilde{p})$, with $\tilde{I}_o=(\tilde{o}+\tilde{o}^\dagger)/\sqrt{2},\,\tilde{J}_o=i(\tilde{o}^\dagger-\tilde{o})/\sqrt{2},\,$ can be written in the following matrix form

$$\dot{\Phi}(t) = \Gamma \Phi(t) + \mathcal{N}(t), \tag{5}$$

where Γ is the drift matrix, given as

$$\Gamma = \begin{pmatrix} -\kappa_a & \Delta_a & 0 & g_a & 0 & 0\\ -\Delta_a & -\kappa_a & -g_a & 0 & 0 & 0\\ 0 & g_a & -\kappa_{\theta_+} & \tilde{\Delta}_{\theta_+} & -G_m & 0\\ -g_a & 0 & -\tilde{\Delta}_{\theta_-} & -\kappa_{\theta_-} & 0 & 0\\ 0 & 0 & 0 & 0 & \omega_b\\ 0 & 0 & 0 & G_m & -\omega_b & -\gamma_b \end{pmatrix}, \quad (6)$$

where $\tilde{\Delta}_{\theta\pm} = \bar{\Delta}_m \pm \Delta_{\theta}$ is the effective detuning of the squeezed magnon drive, including the frequency shift due to magnomechanical interaction, with $\Delta_{\theta} = \Upsilon \sin \theta$ and $\bar{\Delta}_m = \Delta_m + g_m q_s$. Typically, these frequency shifts are small, i.e. $|\bar{\Delta}_m - \Delta_m| \ll \Delta_m$ [5, 51]. Besides, $\kappa_{\theta\pm} = \kappa_m \pm \kappa_{\theta}$ is the effective decay rate of the magnon mode, where $\kappa_{\theta} = \Upsilon \cos \theta$. $G_m = i\sqrt{2}g_m m_s$ is the magnomechanical coupling strength enhanced through coherent driving, where $q_s = -ig_m |m_s|^2/\omega_b^2$. While, m_s is expressed as

$$m_s = \langle m \rangle = \frac{\varkappa_-(i\Delta_a + \kappa_a) + \Upsilon(\Delta_a^2 + \kappa_a^2)e^{i\theta}}{\varkappa_-\varkappa_- - \Upsilon^2(\Delta_a^2 + \kappa_a^2)}\Omega_0, (7)$$

where $\varkappa_{\pm} = (\kappa_a \pm i\Delta_a)(\kappa_m \pm i\bar{\Delta}_m) + g_a^2$. Hence, m_s in Eq.(7) can be expressed as the following form

$$m_s = \frac{\Upsilon e^{i\theta} + i\eta}{\eta^2 - \Upsilon^2} \Omega_0, \tag{8}$$

where $\eta = (g_a^2/\Delta_a) - \bar{\Delta}_m$, when $|\Delta_a|, |\bar{\Delta}_m| \gg \kappa_a, \kappa_m$.

The drift matrix in Eq. (5) is given under the condition $|\Delta_a|, |\tilde{\Delta}_m| \simeq \omega_b \gg \kappa_a, \kappa_m$, which is the optimal condition for quantum correlations in the system [2]. As a result of the linearized dynamics and the Gaussian nature of the quantum noise, its state can be fully described as the steady state of the quantum fluctuations of the system. Indeed, it is characterized by the covariance matrix \mathcal{V} with components $\mathcal{V}_{ij}(t) = \langle \Phi_i(t)\Phi_j(t') + \Phi_j(t')\Phi_i(t) \rangle / 2$. Hence, one can obtain the steady state \mathcal{V} by solving the following Lyapunov equation as

$$\Gamma \mathcal{V} + \mathcal{V}\Gamma^T = -\Lambda, \tag{9}$$

where Λ is the diffusion matrix defined by $\Lambda_{ij}\delta(t'-t) = \langle n_i(t)n_j(t') + n_j(t')n_i(t) \rangle / 2$. It can be rewritten as $\Lambda = \text{diag}[\kappa_a(2\bar{n}_a+1), \kappa_a(2\bar{n}_a+1), \kappa_m(2\bar{n}_m+1), \kappa_m(2\bar{n}_m+1), 0, \gamma_b(2\bar{n}_b+1)]$.

III. NONRECIPROCITY OF THE ENTANGLEMENT

In order to quantify the quantum entanglement among the photon-magnon-phonon modes in the system, we adopt the logarithmic negativity $\mathcal{E}_{\mathcal{N}}$ [52, 53] and the residual angle $\mathcal{R}_{\mathcal{N}}$ [54, 55]. In fact, to investigate the tripartite entanglement, a bona fide quantifier is given by the minimum residual contangle as [56]

$$\mathcal{R}_{\mathcal{N}}^{\min} \equiv \min \left[\mathcal{R}_{\mathcal{N}}^{a|mb}, \mathcal{R}_{\mathcal{N}}^{m|ab}, \mathcal{R}_{\mathcal{N}}^{b|am} \right], \tag{10}$$

where $\mathcal{R}_{\mathcal{N}} \equiv C_{i|jk} - C_{i|j} - C_{i|k}$ denotes the residual contangle, where $C_{\alpha|\beta}$ defines the contangle of the subsystems α and β (β contains one or two modes). Indeed, it satisfies the monogamy of quantum entanglement, namely $C_{i|jk} \geq C_{i|j} + C_{i|k}$. Note that a non-zero minimum residual angle $\mathcal{R}_{\mathcal{N}}^{\min} > 0$ suggests the presence of tripartite entanglement in the system.

Furthermore, to quantitatively represent switchable or nonreciprocal entanglement [34], one should introduce the bidirectional contrast ratio \mathcal{C} for bipartite and tripartite entanglement in nonreciprocal regimes

$$C_{\mathcal{E}} = \frac{|\mathcal{E}_{\mathcal{N}}(>0) - \mathcal{E}_{\mathcal{N}}(<0)|}{\mathcal{E}_{\mathcal{N}}(>0) + \mathcal{E}_{\mathcal{N}}(<0)},$$

$$C_{\mathcal{R}} = \frac{|\mathcal{R}_{\mathcal{N}}(>0) - \mathcal{R}_{\mathcal{N}}(<0)|}{\mathcal{R}_{\mathcal{N}}(>0) + \mathcal{R}_{\mathcal{N}}(<0)}.$$
(11)

Here, $C_{\mathcal{E}}(C_{\mathcal{R}}) = 1$ represents an ideal nonreciprocity. While, $C_{\mathcal{E}}(C_{\mathcal{R}}) = 0$ indicates a complete absence of non-reciprocity for bipartite (tripartite) entanglement.

The physical mechanism behind nonreciprocal entanglement in our system differs significantly to conventional approaches. While basic methods based on Kerr, Sagnac or Barnett effects generally produce simple red

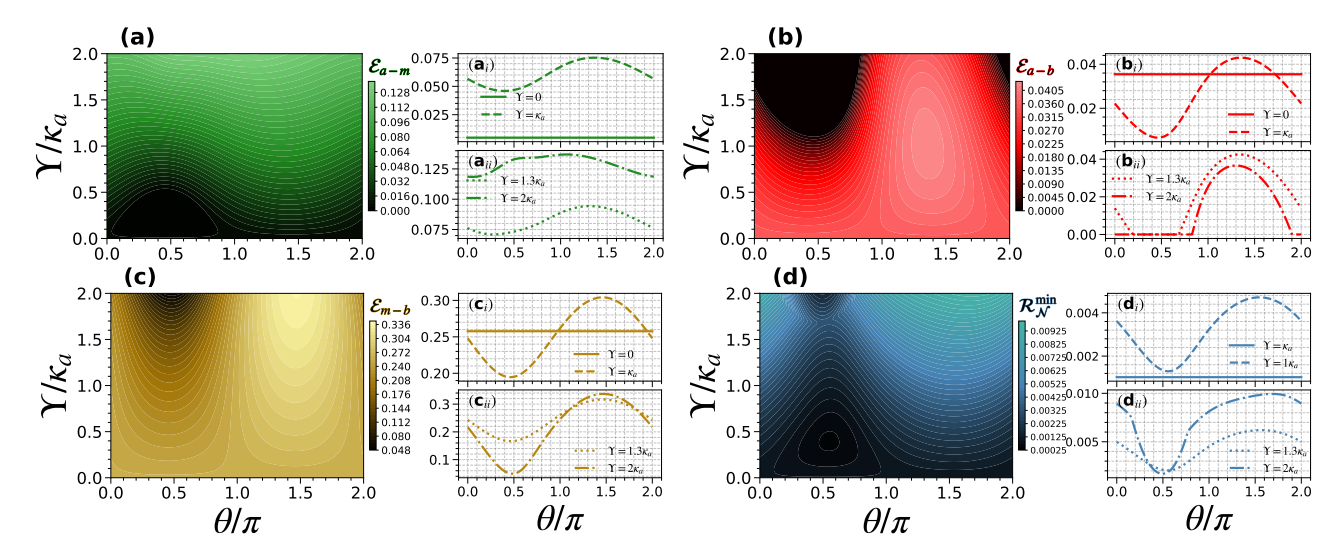


FIG. 2: Density plots of logarithmic negativity: (a) \mathcal{E}_{a-m} (green), (b) \mathcal{E}_{a-b} (red), (c) \mathcal{E}_{m-b} (brown), and (d) the minimum residual contangle $\mathcal{R}_{\mathcal{N}}^{\min}$ (blue), versus the squeezed parameter Υ and phase parameter θ . Moreover, we set $\Upsilon=0$ (solid line) and $\Upsilon=\kappa_a$ (dashed line) in (a_i)-(d_i). Besides, $\Upsilon=1.3\kappa_a$ (dotted line) and $\Upsilon=2\kappa_a$ (dot-dashed line) in (a_{ii})-(d_{ii}). Finally, $\Delta_a=\Delta_m=\omega_b$, T=10mK, while the other parameters are provided in the main text.

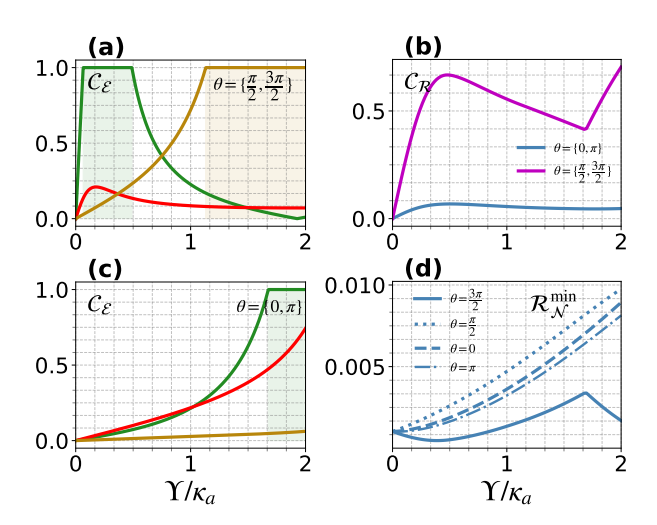


FIG. 3: Bidirectional contrast ratios $C_{\mathcal{E}}^{a-m}$ (green), $C_{\mathcal{E}}^{a-b}$ (red), and $C_{\mathcal{E}}^{m-b}$ (brown) versus the squeezing parameter Υ for (a) $\theta = \{\pi/2, 3\pi/2\}$ and (c) $\theta = \{0, \pi\}$. In figure (b), we plot $\mathcal{C}_{\mathcal{R}}$ versus the squeezing parameter Υ for $\theta = \{\pi/2, 3\pi/2\}$ (purple) and $\theta = \{0, \pi\}$ (blue). (d) is the minimum residual contangle $\mathcal{R}_{\mathcal{N}}^{\min}$ versus the squeezing parameter Υ . The colored vertical stripes represent the ideal nonreciprocal entanglement zones ($\mathcal{C}_{\mathcal{E}} = 1$). The other parameters are the same as in Fig.2.

or blue shifts, magnon squeezing generates a richer structure [31–38]. This mechanism produces simultaneously the effective frequency shifts that depend basically on the amplitude and phase parameters of the squeezing process, while also modifying the magnon decay rate. Note that the results presented here are obtained us-

ing experimentally feasible parameters [1, 2, 5], namely $\omega_m/2\pi=10 {\rm GHz},\ \omega_b/2\pi=10 {\rm MHz},\ \kappa_a/2\pi=3 {\rm MHz},\ \kappa_m=\kappa_a/5,\ G_m/2\pi=g_a/2\pi=4.8 {\rm MHz},\ \gamma_b/2\pi=10^2 {\rm Hz},$ and the temperature T=10 mK (the lowest temperature of a dilution refrigerator). In this situation, $\Delta_a\bar{\Delta}_m\simeq\omega_b^2\gg g_a^2$, where the effective magnomechanical coupling is $G_m\simeq\sqrt{2}g_m(\omega_b+i\Upsilon e^{i\theta})/(\omega_b^2-\Upsilon^2)$ (see Eq. (8)). Indeed, $G_m=4.8 {\rm MHz}$ can be achieved by using a driving magnetic field $H_d\simeq 2.87\times 10^{-5}{\rm T}$ for $\theta=\pi/2,\ g_m=0.2 {\rm Hz}$ [57], and $\Upsilon=1.3\kappa_a$. The results presented are obtained when the system is stable, in accordance with the Routh-Hurwitz criterion [58].

In order to achieve magnon squeezing and observe significant nonreciprocal entanglement, it is essential to drive the magnon mode with a red-detuned microwave field $\Delta_m \simeq \omega_b$, as it effectively cools the vibrational mode close to its quantum ground state. Note that the sign of Δ_{θ} plays a crucial role in the determination of the nonreciprocal entanglement in the system. Effectively, this approach presents several advantages with respect to the other methods. This is according to the fact that it allows to observe a measured variation in detuning by modifying the phase in a positive or negative way, which gives access to variable entanglement and makes it possible to obtain nonreciprocal entanglement. The synergy between phase detuning $(\Delta_{\theta_{+}})$ and dissipation control $(\kappa_{\theta_{\pm}})$ enables directional entanglement enhancement, a unique method unattainable with other effects [31–38], offering freedom in the choice of directional control. Given that Υ is non-negative, the sign of $\Delta_{\theta_{+}}$ and $\kappa_{\theta_{+}}$ depends on the phase parameter indicated in Tab.I.

Fig.2(a) illustrates how the entanglement \mathcal{E}_{a-m} changes during magnon squeezing process with respect to changing the parameters θ and Υ . Indeed, it is

Tab. I: The sign intervals of phase shift and dissipation control parameters.

Signe	$\Delta_{ heta}$	$\kappa_{ heta}$	$(\kappa_{ heta}, \Delta_{ heta})$
> 0 < 0 = 0	$(0, \pi)$ $(\pi, 2\pi)$ $\{0, \pi\}$	$ \begin{pmatrix} 0, & \frac{\pi}{2} \end{pmatrix} \cup \begin{pmatrix} \frac{3\pi}{2}, & 2\pi \end{pmatrix} \\ \begin{pmatrix} \frac{\pi}{2}, & \frac{3\pi}{2} \\ \frac{\pi}{2}, & \frac{3\pi}{2} \end{pmatrix} $	$ \begin{pmatrix} 0, & \frac{\pi}{2} \\ \pi, & \frac{3\pi}{2} \end{pmatrix} $

clear that the entanglement increases progressively with the squeezing amplitude, reaching its maximum for $\Upsilon = 1.3\kappa_a$, confirming the efficiency of the magnetic process. As shown in Fig.2(b), there is a clear decrease in the entanglement \mathcal{E}_{a-b} with a maximum amplitude of 0.04. The non-uniform spatial behavior shows maximum values at some points and zero at symmetric points, revealing a nonreciprocity phenomenon. Moreover, for $\Upsilon = 1.3\kappa_a$, the asymmetry becomes evident, with a maximum at $\theta = 3\pi/2$ and no effect at $\theta = \pi/2$. However, as illustrated in Fig.2(c), the entanglement \mathcal{E}_{m-b} demonstrates a significant intensification, reaching a value of 0.33. Despite maintaining the same spatial behavior as Fig.2(b), the amplitude is significantly amplified, ensuring the preservation of nonreciprocity properties with enhanced efficiency. Finally, in Fig.2(d) shows the tripartite entanglement of the system R_N^{\min} with amplitude 0.05. As with the previous cases, the configuration reproduces the observed amplitude variations, but in a multipartite context, offering a complementary perspective on the quantum correlations of the MM cavity.

Fig.3(a) shows the evolution of nonreciprocity $C_{\mathcal{E}}$ versus Υ between $\theta = \{\pi/2, 3\pi/2\}$. As it is obvious, $C_{\mathcal{E}}^{a-m}$ (green color) and $C_{\mathcal{E}}^{m-b}$ (brown color) maintain high values for strong squeezing parameters ($\Upsilon < 0.5\kappa_a$ for

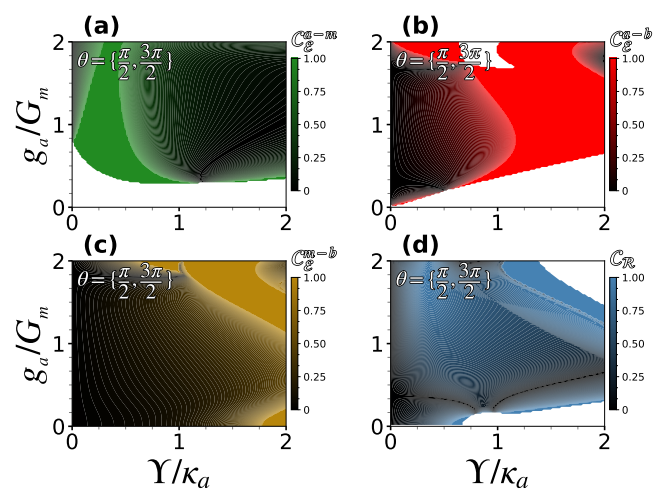


FIG. 4: Density plots of bidirectional contrast ratios (a) $C_{\mathcal{E}}^{a-m}$, (b) $C_{\mathcal{E}}^{a-b}$, (c) $C_{\mathcal{E}}^{m-b}$, and (d) $C_{\mathcal{R}}$, versus the cavity-magnon coupling g_a and the squeezed parameter Υ for $\theta = \{\pi/2, 3\pi/2\}$. The other parameters are the same as in Fig.2.

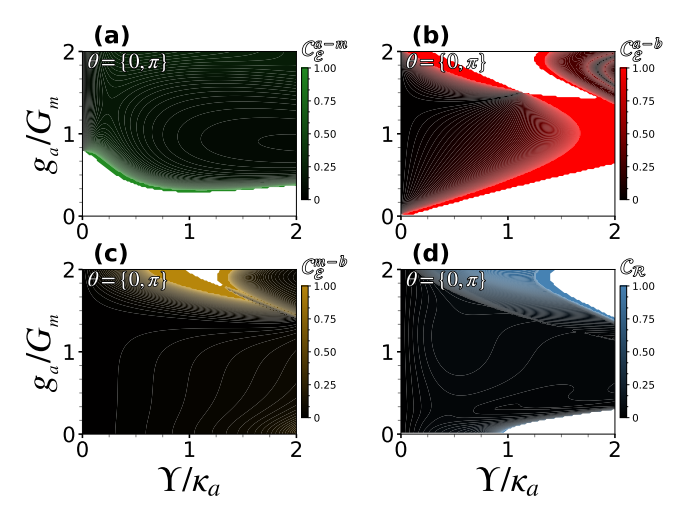


FIG. 5: Density plots of bidirectional contrast ratios (a) $C_{\mathcal{E}}^{a-m}$, (b) $C_{\mathcal{E}}^{a-b}$, (c) $C_{\mathcal{E}}^{m-b}$, and (d) $C_{\mathcal{R}}$, versus the cavity-magnon coupling g_a and the squeezed parameter Υ for $\theta = \{0, \pi\}$. The other parameters are the same as in Fig.2.

 $\mathcal{C}_{\mathcal{E}}^{a-m}$, $\Upsilon > \kappa_a$ for $\mathcal{C}_{\mathcal{E}}^{m-b}$). This indicates an ideal non-reciprocity, namely $\mathcal{C}_{\mathcal{E}} = 1$. Moreover, $\mathcal{C}_{\mathcal{E}}^{a-b}$ (red color) reaches only the amplitude 0.25, revealing a particular sensitivity to squeezing conditions. Fig.3(b) illustrates tripartite entanglement nonreciprocity with reduced amplitudes. Obviously, the bounds of $\mathcal{C}_{\mathcal{R}}$ remain below 0.5 for $\theta = \{\pi/2, 3\pi/2\}$. This indicates a partial reciprocity, while they exceed $\theta = \{0, \pi\}$. These results suggest an orientation-dependent quasi-reciprocal behavior. However, Fig. 3(c) demonstrates the behavior for $\{0, \pi\}$, where $\mathcal{C}_{\mathcal{R}}^{a-m}$ (green) exhibits robust nonreciprocity contrary to $\mathcal{C}_{\mathcal{R}}^{a-b}$ and $\mathcal{C}_{\mathcal{R}}^{m-b}$. This configuration particularly supports the bipartite entanglement $\mathcal{C}_{\mathcal{R}}^{a-m}$. The latter result confirms the decisive influence of the squeezing phase on the correlation asymmetry. Finally, Fig.3(d) reveals a minimum residual contangle with no squeezing parameter, such that all measurements start from the same initial value before progressing differently, indicating nonreciprocity and entanglement enhancement in our system.

Figs.4 and 5 illustrate the impact of two key parameters on nonreciprocal entanglement in the proposed magnomechanical system. These parameters are the cavity-magnon coupling strength g_a and the squeezing parameter Υ . Indeed, the results for a phase squeezing of $\theta = \{\pi/2, 3\pi/2\}$ are presented in Fig.4. As illustrated in Fig.4(a), the nonreciprocal entanglement $\mathcal{C}^{a-m}_{\mathcal{E}}$ attains its maximum values with distinct limits, suggesting that robust cavity-magnon couplings $g_a > G_m$ and a weak squeezing parameters promote ideal nonreciprocity. In addition, Fig.4(b) shows that $\mathcal{C}^{a-b}_{\mathcal{E}}$ demonstrates notable nonreciprocity in some specific regions, particularly when $g_a = G_m$. In this specific case, the nonreciprocity increases with respect to increase the squeezing parameter until reaching ideal nonreciprocity. In Fig.4(c), the ideal nonreciprocity $\mathcal{C}^{m-b}_{\mathcal{E}}$ gives rise

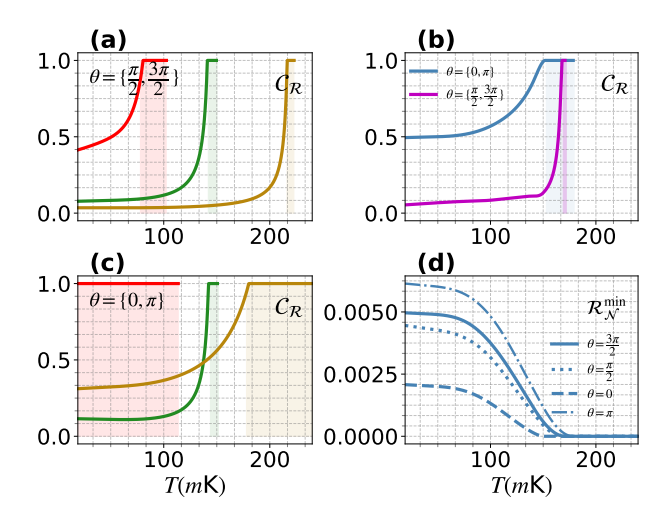


FIG. 6: Bidirectional contrast ratios $C_{\mathcal{E}}^{a-m}$ (green), $C_{\mathcal{E}}^{a-b}$ (red), and $C_{\mathcal{E}}^{m-b}$ (brown) versus the bath temperature T(mK) for (a) $\theta = \{\pi/2, 3\pi/2\}$ and (c) $\theta = \{0, \pi\}$. (b) $C_{\mathcal{R}}$ versus the squeezing parametre Υ for $\theta = \{\pi/2, 3\pi/2\}$ (purple) and $\theta = \{0, \pi\}$ (blue). (d) Minimum residual contangle $\mathcal{R}_{\mathcal{N}}^{\min}$ versus the squeezing parametre Υ . The coloured vertical stripes represent the ideal nonreciprocal entanglement zones. The parameters are the same as in Fig.2.

to large cavity-magnon couplings $g_a > G_m$ and high squeezing parameters. Additionally, in Fig.4(d), the nonreciprocal tripartite entanglement $\mathcal{C}_{\mathcal{R}}$ shows clear parameter limits and optimal performance characteristics. These analysis reveal precise optimal conditions for maximizing nonreciprocity, requiring fine control of the g_a and Υ parameters to achieve the desired performance. The distinct spatial distributions between the different types of entanglement highlight the versatility of the system in adapting the nonreciprorocal behavior to specific coupling configurations.

As shown in Fig.5, the alternative squeezing phase $\theta = \{0, \pi\}$ exhibits different behavior to the previous configuration, namely $\theta = \{\pi/2, 3\pi/2\}$. This results in significant redistributions without reciprocity. Figs. 5(a) and (b) illustrate ideal reciprocity-free regions repositioned towards intermediate values g_a , demonstrating the crucial influence of phase squeezing on optimal zone location. Fig. 5 (c) and (d) show small ideal nonreciprocity regions and exhibit larger critical zones compared to $\theta = \{\pi/2, 3\pi/2\}$. However, a key advantage corresponds to $\theta = \{0, \pi\}$ configuration that allows to ideal nonreciprocity even without impact on the tuning offset. Importantly, the magnetostrictive coupling creates distinct threshold effects, where ideal nonreciprocity only appears above critical coupling strengths and squeezing parameters. However, ideal nonreciprocity becomes more limited in the configuration of $\theta = \{0, \pi\}$.

Fig.6 illustrates the temperature dependence of the nonreciprocity across different phase compression con-

figurations. In fact, Fig.6(a-c) show the nonreciprocity of bipartite and tripartite entanglement C_R versus temperature for the phase configurations $\theta = \{\pi/2, 3\pi/2\},\$ and $\theta = \{0, \pi\}$. Fig.6(a) corresponds to the phase squeezing $\theta = \{\pi/2, 3\pi/2\}$ and reveals ideal nonreciprocity at robust temperatures that varies between 80mK-100mK for $C_{\mathcal{E}}^{a-b}$, 140mK-150mK for $C_{\mathcal{E}}^{a-m}$ and 216mK-223mK for $C_{\mathcal{E}}^{m-b}$. Fig.6(b) shows the same quantity, but in a different phase squeezing configuration, with $\mathcal{C}_{\mathcal{R}}$ (brown line) representing $\theta = \{0, \pi\}$ and $\mathcal{C}_{\mathcal{R}}$ (blue line) corresponding to $\theta = \{\pi/2, 3\pi/2\}$. Indeed, it highlights the distinct temperature thresholds above which nonreciprocity disappears. Fig.6(c), which corresponds to the phase squeezing $\theta = \{0, \pi\}$, shows a wider region of ideal nonreciprocity comparing to $\theta = \{\pi/2, 3\pi/2\}$, with ideal nonreciprocity is observed for $C_{\mathcal{E}}^{a-m}$ when T<114mK. Also, it is observed for $C_{\mathcal{E}}^{a-b}$ when 142mK-151mK, and for $C_{\mathcal{E}}^{m-b}$ when 180mK-200mK. Fig.6(d) shows the minimum residual contangle $R_{\mathcal{N}}^{min}$, which decreases monotonically with increasing temperature for all sets of parameters (represented by different styles of lines corresponding to the phase squeezing), indicating a degradation of the quantum squeezing effects.

Note that the validity of all the above figures depends on the condition that the number of magnonic excitations $\langle m^{\dagger}m\rangle \ll 2N_0s = 5N_0$, where $s = \frac{5}{2}$ as montioned in sec.II. For a 250μ m-diameter YIG sphere, the number of spins $N_0 = 3.5 \times 10^{16}$. $|\langle m \rangle| \simeq 1.69 \times 10^7$ corresponds to the MM coupling $G_m/2\pi = 4.8 \text{MHz}$, $\theta = \pi/2$ and Rabi frequency $\Omega_0 \simeq 1.48 \times 10^{15} \mathrm{Hz}$, which leads to $|\langle m^\dagger m \rangle| \simeq 2.88 \times 10^{14} \ll 5 N_0 = 1.8 \times 10^{17}$. This condition is, therefore, satisfied. High pumping power is adopted for magnon modes, which can introduce unwanted nonlinearity due to the nonlinear Kerr term $\mathcal{K}m^{\dagger}mm^{\dagger}m$ in the Hamiltonian [59, 60]. To ensure that the K remains negligible, the $K |\langle m \rangle|^3 \ll \Omega_0$ condition must be satisfied. The positive Kerr coefficient varies inversely proportional to the sphere volume, for what we use a 250μ m-diameter YIG sphere, $\mathcal{K}/2\pi = 6.4 \mathrm{nHz}$. With the parameters used in the paper, $\mathcal{K}|\langle m\rangle|^3 = 1.96 \times 10^{14} \text{Hz} \ll \Omega_0$, validating that linearization provides a good approximation. Hence, the nonlinear effects remain negligible.

Finally, let discuss how we verify the magnon squeezing and examine the intrinsic phase-space fluctuations for the quadrature pair $\{\tilde{X}_m, \tilde{Y}_m\}$. Then, we reconstruct the Wigner function $\mathcal{W}(\varphi)$ for the magnon mode, which provides a full representation of its Gaussian quantum state and allows direct visualization of the squeezing phenomenon. Indeed, the Wigner function is expressed as

$$W(\varphi) = \frac{\exp(-(\varphi \tilde{\mathcal{V}} \varphi^{\dagger})/2)}{\pi^2 \sqrt{\det \mathcal{V}}},$$
 (12)

where φ is the quadrature vector and $\tilde{\mathcal{V}}$ is the magnon quadrature sub-covariance matrix \mathcal{V} . As shown in Fig.7, the Wigner function displays an elliptical form, indi-

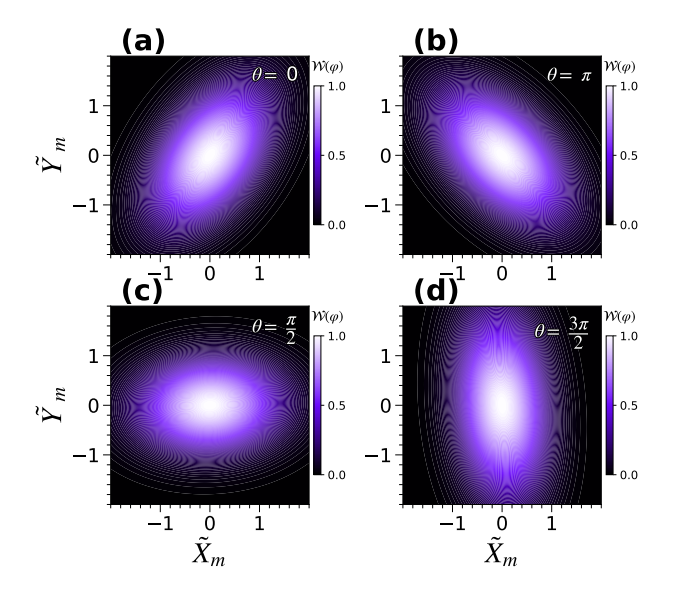


FIG. 7: Density plots of the reconstructed Wigner function $\mathcal{W}(\varphi)$ for quadrature magnon mode pairs at different values of squeezing phase: (a) $\theta=0$, (b) $\theta=\pi$, (c) $\theta=\pi/2$, and (d) $\theta=3\pi/2$ These configurations are used to obtain nonreciprocal entanglement with parameters $\Delta_a=\Delta_m=\omega_b, \Upsilon=1.3\kappa_a, T=10\text{mK}$, and other parameters are listed in the main text.

cating the presence of a squeezed magnon mode for different squeezed phases used to find the nonricprocity of entanglement to confirm that we remain in the squeezed magnon framework. These density diagrams of the Wigner function provide direct visual evidence of the magnon squeezing obtained and confirm the effectiveness of our approach in obtaining nonreciprocity of entanglement with control of directional magnon squeezing.

IV. CONCLUSION

In conclusion, we have presented a novel approach to generate and control bipartite and tripartite nonreciprocal macroscopic entanglement in a magnomechanical cavity using squeezed magnons. Contrary to the previous conventional effect-based methods [31– 38, our approach exploited the combination of phasedependent frequency shifts and tunable dissipation used to achieve directional entanglement via the amplitude and phase control of magnon squeezing. All these goals are achieved used for all experimentally accessible parameters. Our main results showed that the squeezing phase switched the nonreciprocal directionality, offering an advantage for precise control of nonreciprocal entanglement. Moreover, we established by taking various cases that this approach enabled ideal nonreciprocity using the optimal conditions for the cavity-magnon coupling and the bath temperature. Importantly, we verified the observation of squeezed magnons for all possible squeezing phases used to achieve nonreciprocity, thus confirming the quantum validity of our approach. The squeezed magnon states obtained in a massive system constitute genuine macroscopic quantum states. These state underline their potential for probing quantum effects at macroscopic scales [61]. Therefore, our findings highlight a new mechanism for the generation of nonreciprocal quantum entanglement, and open up promising prospects for the development of robust quantum devices suitable for quantum information networks based on magnonic hybrid systems, as well as in the field of single photon detection [62, 63].

Zuo, X., Fan, Z. Y., Qian, H., Ding, M. S., Tan, H., Xiong, H., Li, J. (2024). Cavity magnomechanics: from classical to quantum. New Journal of Physics, 26(3), 031201.

^[2] Li, J., Zhu, S. Y., Agarwal, G. S. (2018). Magnon-photonphonon entanglement in cavity magnomechanics. Physical review letters, 121(20), 203601.

^[3] Zhang, Z., Scully, M. O., Agarwal, G. S. (2019). Quantum entanglement between two magnon modes via Kerr nonlinearity driven far from equilibrium. Physical Review Research, 1(2), 023021.

^[4] Yu, M., Shen, H., Li, J. (2020). Magnetostrictively induced stationary entanglement between two microwave fields. Physical Review Letters, 124(21), 213604.

^[5] Zhang, X., Zou, C. L., Jiang, L., Tang, H. X. (2016). Cavity magnomechanics. Science advances, 2(3), e1501286.

^[6] Osada, A., Hisatomi, R., Noguchi, A., Tabuchi, Y., Yamazaki, R., Usami, K., Nakamura, Y. (2016). Cavity optomagnonics with spin-orbit coupled photons. Physical review letters, 116(22), 223601.

^[7] Zhang, X., Zhu, N., Zou, C. L., Tang, H. X. (2016). Optomagnonic whispering gallery microresonators. Physical review letters, 117(12), 123605.

^[8] Asano, M., Matsumoto, H., Hayashi, M., Hatanaka, D. (2023). Cavity magnomechanical coupling with coupled magnon modes in a synthetic antiferromagnet. Physical Review B, 108(6), 064415

^[9] Heyroth, F., Hauser, C., Trempler, P., Geyer, P., Syrowatka, F., Dreyer, R., Schmidt, G. (2019). Monocrystalline freestanding three-dimensional yttrium-irongarnet magnon nanoresonators. Physical Review Applied, 12(5), 054031

^[10] Imara, Z., Castillo, I. P., Anouz, K. E., Allati, A. E. (2025). Tunable Entangling and Steering of Ferrimagnetic Magnons via an OptoMagnoMechanical Ring. arXiv preprint arXiv:2504.13117.

^[11] Imara, Z., El Anouz, K., Saif, F., El Allati, A. (2024). Quantum effect in a hybrid bose-einstein condensate optomagnomechanical system. Journal of Physics B: Atomic, Molecular and Optical Physics, 57(23), 235501.

^[12] Serga, A. A., Chumak, A. V., Hillebrands, B. (2010). YIG magnonics. Journal of Physics D: Applied Physics, 43(26), 264002.

^[13] Xu, G. T., Zhang, M., Wang, Z. Y., Wang, Y., Liu, Y. X., Shen, Z., Dong, C. H. (2023). Ringing spectroscopy in the magnomechanical system. Fundamental Research, 3(1), 45-49

- [14] Tang, J., Shen, H. Z. (2024). Non-Markovian frequency conversion between optical and microwave photons with magnetomechanical transduction. Physical Review A, 110(4), 043706.
- [15] Li, J., Wang, Y. P., Wu, W. J., Zhu, S. Y., You, J. Q. (2021). Quantum network with magnonic and mechanical nodes. PRX Quantum, 2(4), 040344
- [16] Huebl, H., Zollitsch, C. W., Lotze, J., Hocke, F., Greifenstein, M., Marx, A., Goennenwein, S. T. (2013). High cooperativity in coupled microwave resonator ferrimagnetic insulator hybrids. Physical Review Letters, 111(12), 127003.
- [17] Zhang, D., Luo, X. Q., Wang, Y. P., Li, T. F., You, J. Q. (2017). Observation of the exceptional point in cavity magnon-polaritons. Nature communications, 8(1), 1368.
- [18] Asjad, M., Li, J., Zhu, S. Y., You, J. Q. (2023). Magnon squeezing enhanced ground-state cooling in cavity magnomechanics. Fundamental Research, 3(1), 3-7.;
- [19] Lu, T. X., Xiao, X., Chen, L. S., Zhang, Q., Jing, H. (2023). Magnon-squeezing-enhanced slow light and secondorder sideband in cavity magnomechanics. Physical Review A, 107(6), 063714.
- [20] Li, J., Wang, Y. P., You, J. Q., Zhu, S. Y. (2023). Squeezing microwaves by magnetostriction. National Science Review, 10(5), nwac247.
- [21] Yu, M., Shen, H., Li, J. (2020). Magnetostrictively induced stationary entanglement between two microwave fields. Physical Review Letters, 124(21), 213604.
- [22] Qian, H., Zuo, X., Fan, Z. Y., Cheng, J., Li, J. (2024). Strong squeezing of microwave output fields via reservoir-engineered cavity magnomechanics. Physical Review A, 109(1), 013704.
- [23] Guo, Q., Cheng, J., Tan, H., Li, J. (2023). Magnon squeezing by two-tone driving of a qubit in cavity-magnon-qubit systems. Physical Review A, 108(6), 063703.
- [24] Fan, Z. Y., Zhu, H. B., Li, H. T., Li, J. (2024). Magnon squeezing via reservoir-engineered optomagnomechanics. APL Photonics, 9(10).
- [25] Li, J., Zhu, S. Y., Agarwal, G. S. (2019). Squeezed states of magnons and phonons in cavity magnomechanics. Physical Review A, 99(2), 021801.
- [26] Imara, Z., El Anouz, K., El Allati, A. (2024). Engineering and control of the entanglement for four Magnon modes inside two microwave cavities. Journal of Physics B: Atomic, Molecular and Optical Physics, 57(18), 185501.
- [27] Jiao, Y. F., Zhang, S. D., Zhang, Y. L., Miranowicz, A., Kuang, L. M., Jing, H. (2020). Nonreciprocal optomechanical entanglement against backscattering losses. Physical Review Letters, 125(14), 143605.
- [28] Malykin, G. B. (2000). The Sagnac effect: correct and incorrect explanations. Physics-Uspekhi, 43(12), 1229.
- [29] Maayani, S., Dahan, R., Kligerman, Y., Moses, E., Hassan, A. U., Jing, H., Carmon, T. (2018). Flying couplers above spinning resonators generate irreversible refraction. Nature, 558(7711), 569-572.
- [30] Lu, T. X., Li, B., Wang, Y., Wang, D. Y., Xiao, X., Jing, H. (2024). Directional quantum-squeezing-enabled nonreciprocal enhancement of entanglement. Physical Review Applied, 22(6), 064001.
- [31] Ullah, M., Mikki, S. (2024). Nonreciprocal microwave field transmission in a quantum magnomechanical system controlled by magnetostriction and Kerr nonlinearities. Physical Review B, 109(21), 214303.
- [32] Chen, J., Fan, X. G., Xiong, W., Wang, D., Ye, L. (2024). Nonreciprocal photon-phonon entanglement in Kerrmodified spinning cavity magnomechanics. Physical Review A, 109(4), 043512.
- [33] Xu, Y., Liu, J. Y., Liu, W., Xiao, Y. F. (2021). Nonreciprocal phonon laser in a spinning microwave magnomechanical system. Physical Review A, 103(5), 053501.
- [34] Chen, J., Fan, X. G., Xiong, W., Wang, D., Ye, L. (2023). Nonreciprocal entanglement in cavity-magnon optomechanics. Physical Review B, 108(2), 024105.

- [35] Fan, Z. Y., Zuo, X., Li, H. T., Li, J. (2024). Nonreciprocal entanglement in cavity magnomechanics exploiting chiral cavity-magnon coupling. arXiv preprint arXiv:2401.02280.
- [36] Yang, G., Guan, S. Y., Han, X., Wang, T., Zhang, S., Wang, H. F. (2025). Chiral Coupling-Enabled Optical Nonreciprocity in a Cavity Magnomechanical System. Advanced Quantum Technologies, 2400702.
- [37] Lu, T. X., Li, Z. S., Chen, L. S., Wang, Y., Xiao, X., Jing, H. (2025). Nonreciprocal entanglement in cavity magnomechanics via the Barnett effect. Physical Review A, 111(1), 013713.
- [38] Ge, P. C., Yu, Y., Wu, H. T., Han, X., Wang, H. F., Zhang, S. (2025). Nonreciprocal bipartite and tripartite entanglement in cavity-magnon optomechanics via the Barnett effect. Scientific Reports, 15(1), 7937.
- [39] Potts, C. A., Varga, E., Bittencourt, V. A., Kusminskiy, S. V., Davis, J. P. (2021). Dynamical backaction magnomechanics. Physical Review X, 11(3), 031053.
- [40] Shen, R. C., Li, J., Fan, Z. Y., Wang, Y. P., You, J. Q. (2022). Mechanical bistability in Kerr-modified cavity magnomechanics. Physical Review Letters, 129(12), 123601.
- [41] Kittel, C. (1958). Interaction of spin waves and ultrasonic waves in ferromagnetic crystals. Physical Review, 110(4), 836.
- [42] Tabuchi, Y., Ishino, S., Ishikawa, T., Yamazaki, R., Usami, K., Nakamura, Y. (2014). Hybridizing ferromagnetic magnons and microwave photons in the quantum limit. Physical review letters, 113(8), 083603.
- [43] Zhang, X., Zou, C. L., Jiang, L., Tang, H. X. (2014). Strongly coupled magnons and cavity microwave photons. Physical review letters, 113(15), 156401.
- [44] Wang, Y. P., Zhang, G. Q., Zhang, D., Li, T. F., Hu, C. M., You, J. Q. (2018). Bistability of cavity magnon polaritons. Physical review letters, 120(5), 057202.
- [45] Wang, Y. P., Zhang, G. Q., Zhang, D., Luo, X. Q., Xiong, W., Wang, S. P., You, J. Q. (2016). Magnon Kerr effect in a strongly coupled cavity-magnon system. Physical Review B, 94(22), 224410.
- [46] Xiong, H. (2023). Magnonic frequency combs based on the resonantly enhanced magnetostrictive effect. Fundamental Research, 3(1), 8-14.
- [47] Kamra, A., Belzig, W. (2016). Super-Poissonian shot noise of squeezed-magnon mediated spin transport. Physical review letters, 116(14), 146601.
- [48] Genes, C., Vitali, D., Tombesi, P., Gigan, S., Aspelmeyer, M. (2008). Ground-state cooling of a micromechanical oscillator: Comparing cold damping and cavity-assisted cooling schemes. Physical Review A—Atomic, Molecular, and Optical Physics, 77(3), 033804.
- [49] Drummond, P. D., Gardiner, C. W. (1980). Generalised P-representations in quantum optics. Journal of Physics A: Mathematical and General, 13(7), 2353.
- [50] Benguria, R., Kac, M. (1981). Quantum langevin equation. Physical review letters, 46(1), 1.
- [51] Kong, C., Wang, B., Liu, Z. X., Xiong, H., Wu, Y. (2019). Magnetically controllable slow light based on magnetostrictive forces. Optics express, 27(4), 5544-5556.
- [52] Vidal, G., Werner, R. F. (2002). Computable measure of entanglement. Physical Review A, 65(3), 032314.
- [53] Plenio, M. B. (2005). Logarithmic negativity: a full entanglement monotone that is not convex. Physical review letters, 95(9), 090503.
- [54] Adesso, G., Illuminati, F. (2006). Continuous variable tangle, monogamy inequality, and entanglement sharing in Gaussian states of continuous variable systems. New Journal of Physics, 8(1), 15.
- [55] Adesso, G., Illuminati, F. (2007). Entanglement in continuous-variable systems: recent advances and current perspectives. Journal of Physics A: Mathematical and Theoretical, 40(28), 7821.

- [56] Coffman, V., Kundu, J., Wootters, W. K. (2000). Distributed entanglement. Physical Review A, 61(5), 052306.
- [57] We choose a higher magnon-phonon coupling value g_m than that given in [5]. This higher coupling reduces the pumping power required and avoids undesirable non-linear effects. It is possible that smaller YIG spheres could achieve these coupling values [2]. As well, the cavity-magnon coupling g_a can be much more important than g_m , as shown in [25].
- [58] DeJesus, E. X., Kaufman, C. (1987). Routh-Hurwitz criterion in the examination of eigenvalues of a system of non-linear ordinary differential equations. Physical Review A, 35(12), 5288.
- [59] Wang, Y. P., Zhang, G. Q., Zhang, D., Luo, X. Q., Xiong, W., Wang, S. P., You, J. Q. (2016). Magnon Kerr effect in a strongly coupled cavity-magnon system. Physical Review B,

- **94**(22), 224410.
- [60] Wang, Y. P., Zhang, G. Q., Zhang, D., Li, T. F., Hu, C. M., You, J. Q. (2018). Bistability of cavity magnon polaritons. Physical review letters, 120(5), 057202.
- [61] The magnon mode in a 250μ m-diameter YIG sphere consists of a large number of spins (about 3.5×10^{16} spins), and is considered to operate on a macroscopic scale sufficient to be identified as a macroscopic quantum state.
- [62] Nunnenkamp, A., Børkje, K., Girvin, S. M. (2011). Single-photon optomechanics. Physical review letters, 107(6), 063602.
- [63] Vitali, D., Gigan, S., Ferreira, A., Böhm, H. R., Tombesi, P., Guerreiro, A., Aspelmeyer, M. (2007). Optomechanical entanglement between a movable mirror and a cavity field. Physical review letters, 98(3), 030405.